



HAL
open science

An approach to the modeling of viscoelastic damage. Application to the long-term creep of gypsum rock materials

Boumediene Nedjar, Robert Le Roy

► **To cite this version:**

Boumediene Nedjar, Robert Le Roy. An approach to the modeling of viscoelastic damage. Application to the long-term creep of gypsum rock materials. *International Journal for Numerical and Analytical Methods in Geomechanics*, 2012, 19 p. 10.1002/nag.1138 . hal-00668051

HAL Id: hal-00668051

<https://enpc.hal.science/hal-00668051>

Submitted on 9 Feb 2012

HAL is a multi-disciplinary open access archive for the deposit and dissemination of scientific research documents, whether they are published or not. The documents may come from teaching and research institutions in France or abroad, or from public or private research centers.

L'archive ouverte pluridisciplinaire **HAL**, est destinée au dépôt et à la diffusion de documents scientifiques de niveau recherche, publiés ou non, émanant des établissements d'enseignement et de recherche français ou étrangers, des laboratoires publics ou privés.

An approach to the modelling of viscoelastic-damage. Application to the long-term creep of gypsum rock materials

B. Nedjar* and R. Le Roy

Université Paris-Est, Laboratoire Navier (ENPC/IFSTTAR/CNRS), Ecole des Ponts ParisTech, 6 et 8 avenue Blaise Pascal, 77455 Marne-la-Vallée, France

SUMMARY

A three-dimensional phenomenological model is developed to describe the long-term creep of gypsum rock materials. The approach is based on the framework of continuum damage mechanics where coupling with viscoelasticity is adopted. Specifically, a local damage model based on the concept of yield surface is proposed and deeply investigated. And among the many possibilities, we choose in this work its coupling with a generalized Kelvin-Voigt rheological model to formulate the whole behaviour. Long-term as well as short-term relaxation processes can be integrated in the model by means of as many as necessary viscoelastic processes. The numerical discretization is described for an easy integration within a finite element procedure. Finally, a set of numerical simulations is given to show the possibilities of the presented model. It shows good agreement with some experimental results found in the literature. Copyright © 2011 John Wiley & Sons, Ltd.

Received . . .

KEY WORDS: Gypsum rock; Viscoelasticity; Continuum damage; Tertiary creep; Finite element method

1. INTRODUCTION

In this paper, the attention is focused on the long-term behaviour of gypsum rock materials. In fact, creep in natural gypsum rocks is one of the major phenomena at the origin of degradations in underground mines. It is then of interest to construct life-time predictive tools within a phenomenological modelling framework.

Typically, the uniaxial creep response of natural gypsum rock under compressive loads is characterized by three phases as shown in Figure 1 (after [1]). A first transitory phase of creep is followed by a secondary (almost) steady state phase. The duration of these phases is strongly dependent on the load level. And for loads beyond a certain value, a tertiary creep phase appears which quickly leads to failure. Below that loading value, no tertiary phase appears and the material apparently provides an endurance domain, *i.e.* a domain in the stress space such that the strains reach

*Correspondence to: boumediene.nedjar@enpc.fr, Tel. +33-1-64153715

asymptotic values under creep tests. However, the limiting duration of laboratory experimental tests does not always permit to state the existence of such a domain.

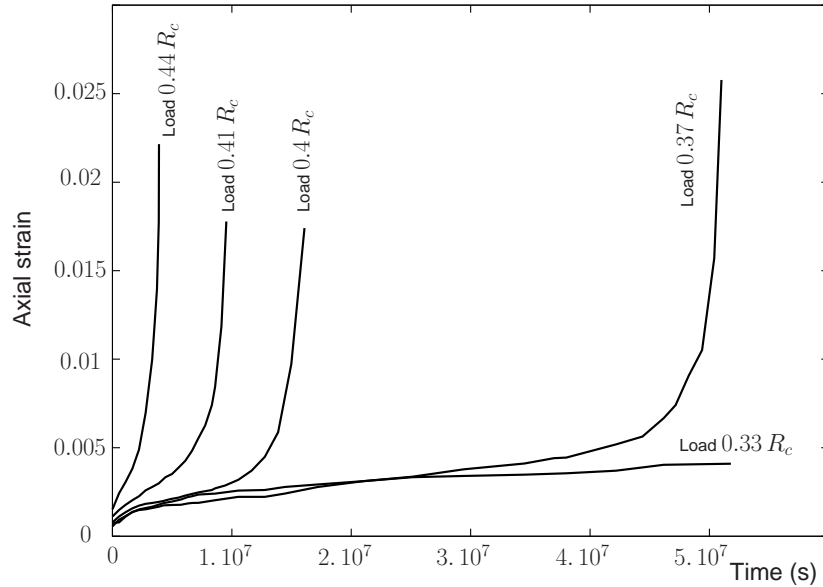


Figure 1. Typical uniaxial creep curves for a saturated saccharoid gypsum rock (after [1]). Each curve corresponds to a load level with respect to the pic load R_c in compression.

There exists different approaches in the literature to model the natural gypsum rock material such as in [2]. In this latter, the approach is based on a viscoplastic model coupled to continuum damage. In fact, viscoplasticity has been intensively used to model rock salt materials that appear to be geologically similar to gypsum rock, see for example [3, 4] for the modelling of rock salt.

On the other hand, creep in civil engineering materials has been widely described by means of viscoelasticity, see for example [5]. Moreover, there exist models where viscoelasticity has been coupled to damage for a variety of materials, see for example [6, 7]. In particular, viscoelastic-damage has been coupled to calcium leaching in [8] to model the long-term creep of a leached concrete.

In this paper, we choose to describe the typical behavior described above by means of a viscoelastic-damage constitutive model where the framework of the continuum damage mechanics is used to model the material degradation. The viscoelastic-damage law adopted here is characterized by means of an internal variable model and it constitutes the simplest form where damage is coupled to elasticity. We write

$$\boldsymbol{\sigma} = (1 - D) \mathbf{C} : (\boldsymbol{\varepsilon} - \boldsymbol{\varepsilon}^v) \quad (1)$$

where $\boldsymbol{\sigma}$ and $\boldsymbol{\varepsilon}$ are the second order stress and strain tensors, respectively, \mathbf{C} is the fourth-order Hooke's elasticity tensor, the scalar D is the internal damage variable with value 0 when the material is undamaged and value 1 when the material is completely damaged. And where the strain-like internal variable $\boldsymbol{\varepsilon}^v$ is the viscous part of the strain tensor. Isotropy is assumed throughout this paper. In (1) and in all what follows, the double dot symbol $:$ denotes the double tensor contraction.

As for the damage variable D , the internal variable ε^v is not accessible to direct observation and, moreover, it can in turn be the sum of as many as necessary internal contributions ε_i^v , *i.e.*

$$\varepsilon^v = \sum_{i=1}^{\ell} \varepsilon_i^v \quad (2)$$

where the $i = 1, \dots, \ell$ hidden tensor variables ε_i^v characterize viscoelastic processes with corresponding relaxation times $\tau_i \in (0, \infty)$, $i = 1, \dots, \ell$. Of course, a viscoelastic description based solely via external variables is also possible. The way all these internal variables evolve is motivated by the one-dimensional rheological model of Section 2.

The rest of the paper is organized as follows. In Section 3, the one-dimensional rheological model of Section 2 is extended to the three-dimensional case. A model example is given and its numerical integration within the finite element method is detailed in Section 4. Then a set of representative numerical examples are given and discussed in Section 5. And Finally, conclusions are drawn in Section 6.

2. MOTIVATION. ONE-DIMENSIONAL RHEOLOGICAL MODEL

In order to describe the way the viscoelastic and damage processes evolve, it is necessary to specify complementary equations that govern the evolution of the internal variables ε_i^v , $i = 1, \dots, \ell$ and D . This is motivated in this section through a one-dimensional study.

2.1. An effective characterization of viscoelasticity

The rheological model of Figure 2 displays both relaxation and creep behavior. It consists of a free spring on one end and an arbitrary number ℓ of Kelvin elements arranged in series. The stiffnesses of the free spring and the i -spring elements are $\bar{E} > 0$ and $\bar{E}_i > 0$, $i = 1, \dots, \ell$, respectively. And the viscosity of the i -dashpot elements are specified by the material constants $\bar{\eta}_i > 0$, $i = 1, \dots, \ell$. For the sake of simplicity, we suppose in this model that all these elastic and viscoelastic moduli result from the same damage coupling. That is

$$\bar{E} = (1 - D) E, \quad \bar{E}_i = (1 - D) E_i \quad \bar{\eta}_i = (1 - D) \eta_i \quad i = 1, \dots, \ell, \quad (3)$$

where E and (E_i, η_i) , $i = 1, \dots, \ell$, are the corresponding undamaged moduli.

Now the governing equations for the generalized Kelvin-Voigt model depicted in Figure 2 are derived by elementary considerations. Let σ be the stress applied to the whole model and ε be the external variable which measures the total strain. The stress on each i -spring is $\bar{E}_i \varepsilon_i^v$, and the stress on each corresponding i -dashpot is given by the linear relation $\bar{\eta}_i \dot{\varepsilon}_i^v$, where the upper dot ($\dot{}$) is the time derivative. Hence, on the one hand, the resultant stress in each i -Kelvin element (an i -spring in parallel with an i -dashpot) is the sum $\bar{E}_i \varepsilon_i^v + \bar{\eta}_i \dot{\varepsilon}_i^v$. And on the other hand, since the strain on the free spring is $\varepsilon - \varepsilon^v$, where $\varepsilon^v = \sum_{i=1, \ell} \varepsilon_i^v$, the stress on this spring is given by $\bar{E} (\varepsilon - \varepsilon^v)$.

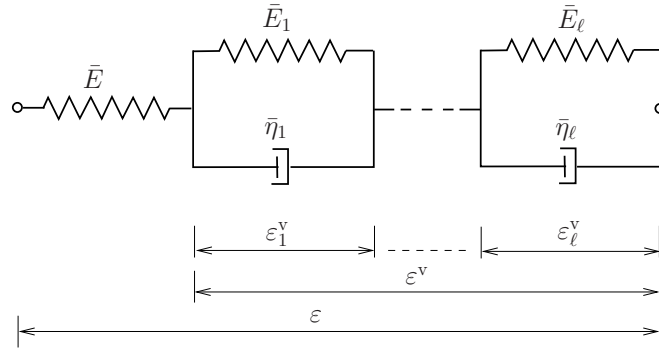


Figure 2. One-dimensional rheological model.

The free spring and all the ℓ Kelvin elements being connected in series, then by equilibrium the stress is found to be given by any of the following ℓ equations

$$\sigma = \bar{E}(\varepsilon - \varepsilon^v) = \bar{E}_i \varepsilon_i^v + \bar{\eta}_i \dot{\varepsilon}_i^v, \quad i = 1, \dots, \ell \quad (4)$$

where no sum on the indices i is assumed.

Denoting by $\tau_i = \bar{\eta}_i / \bar{E}_i \equiv \eta_i / E_i > 0$, $i = 1, \dots, \ell$ the relaxation times, and by $\omega_i > 0$ $i = 1, \dots, \ell$ the stiffness factors such that $\bar{E}_i = \bar{E} / \omega_i$, or equivalently $E_i = E / \omega_i$ by (3), (4)₂ implies the important ℓ evolution equations

$$\dot{\varepsilon}_i^v + \frac{1 + \omega_i}{\tau_i} \varepsilon_i^v + \frac{\omega_i}{\tau_i} \sum_{j=1, j \neq i}^{\ell} \varepsilon_j^v = \frac{\omega_i}{\tau_i} \varepsilon, \quad i = 1, \dots, \ell \quad (5)$$

for the strain-like internal variables ε_i^v , $i = 1, \dots, \ell$. Now in order to describe the way the damage process evolves, it is necessary to specify more complementary equations that govern this time the evolution of the damage internal variable D . This is discussed in the following.

2.2. A strain-based characterization of damage

It is physically essential to take into account both the instantaneous and the delayed deformations in the definition of quantities that drive the damage evolution to, among others, describe the variability of the secondary plateau-like creep phase duration. To this end, the crucial idea underlining the continuum damage model presented in this work is the hypothesis that damage in the material is in fact directly linked to the history of the *total* strains. Attention is still focused here on the one-dimensional case, but later on, these ideas will be extended to the three-dimensional formulation.

To characterize the progressive degradation of the mechanical properties within the continuum damage mechanics' framework, we choose a damage criterion formulated in strain space as

$$g(D; \varepsilon) = (1 - D)^m S(\varepsilon) - W \leq 0 \quad (6)$$

where W is the initial damage threshold and $S(\varepsilon)$ is the driving source of damage which depends solely on the total strain ε . W and S are expressed here in terms of volumetric energies [Nm/m^3].

And the *up to now constant* dimensionless exponent parameter $m > 0$ controls the hardening or the softening material response as will be discussed below.

We next define the evolution of the damage variable D by the rate equation

$$\dot{D} = \delta \quad (7)$$

where δ is the damage consistency parameter that defines the standard damage loading/unloading conditions

$$\delta \geq 0, \quad g(D; \varepsilon) \leq 0, \quad \delta g(D; \varepsilon) = 0. \quad (8)$$

This model is no more than the local version of the gradient damage model presented in [9, 10]. If $g(D; \varepsilon) < 0$, the damage criterion is not satisfied and condition (8)₃ gives $\delta = 0$, hence the damage rule (7) implies that $\dot{D} = 0$ and no further damage takes place. If, on the other hand, $\delta > 0$; that is further damage is taking place, (8)₃ now implies $g(D; \varepsilon) = 0$. In this event the value of δ is determined by the damage consistency condition $\dot{g}(D; \varepsilon) = 0$ which, in our case, gives

$$\delta \equiv \dot{D} = \frac{1-D}{m S(\varepsilon)} \dot{S}(\varepsilon). \quad (9)$$

This latter has a form that matches the general framework proposed in [11]. Now to gain further insight into the nature of the present damage model, let us express in rate form the one-dimensional elastic-damage version of (1): $\sigma = (1-D) E\varepsilon$, when only *instantaneous* damage takes place and in the absence of any viscous strains, *i.e.* with $\varepsilon^v = \dot{\varepsilon}^v = 0$. And, moreover, let the driving source of damage be given for simplicity by the effective strain energy: $S(\varepsilon) = 1/2 E\varepsilon^2$ which implies $\dot{S}(\varepsilon) = E\varepsilon\dot{\varepsilon}$, both these latter quantities to be replaced in the expression (9). One obtains then

$$\dot{\sigma} = (1-D) E\dot{\varepsilon} - \dot{D} E\varepsilon \equiv (1-D) \left\{ 1 - \frac{2}{m} \right\} E\dot{\varepsilon}. \quad (10)$$

It is a well known theoretical result that the tangent modulus is positive for a hardening material response, and is negative in the case of softening. Then, as $(1-D) \geq 0$, the sign of the tangent modulus deduced from the rate form (10) depends solely on the value of the exponent parameter m . We then conclude that, in the present form, the elastic-damage model exhibits pure hardening for $m > 2$, or pure softening for $m < 2$.

However, for geomaterials in general and for rock-like materials in particular, the behavior in compression is characterized by a hardening response when damage initiates until a pic load is reached, and then is followed by a material softening until complete degradation. Hence, to take into account those facts, the exponent material parameter m should not be kept constant but must be variable. In this work, we choose to make it damage-dependent through the following form

$$m(D) = m_1 (1-D)^{m_2} + m_3, \quad (11)$$

with $m_1 \geq 0$, $m_2 > 0$ and $m_3 > 0$ being from now new material parameters. That is, when damage initiates ($D \approx 0$), one has $m \approx m_1 + m_3$, and m tends to m_3 when D approaches complete degradation, *i.e.* when $D \rightarrow 1$. Hence, for instance, choosing the parameters m_1 and m_3 such that $m_1 + m_3 > 2$ with $m_3 < 2$ permits to cover both the hardening and softening stages of the material

response. The convenient parameter m_2 controls the rate at which the transition from hardening to softening is achieved. Also, notice that for $m_1 = 0$, the original model with constant exponent parameter ($m \equiv m_3$) is reached.

3. THREE-DIMENSIONAL EVOLUTION EQUATIONS

For the viscoelastic part of the material behavior, we motivate the evolution equations for the three-dimensional deformation by reference to the relationship (5). An obvious choice of appropriate evolution equations for the internal tensor variables ε_i^y is given by

$$\dot{\varepsilon}_i^y + \frac{1+\omega_i}{\tau_i} \mathbb{N} : \varepsilon_i^y + \frac{\omega_i}{\tau_i} \sum_{j=1, j \neq i}^{\ell} \mathbb{N} : \varepsilon_j^y = \frac{\omega_i}{\tau_i} \mathbb{N} : \varepsilon, \quad i = 1, \dots, \ell \quad (12)$$

where τ_i , $i = 1, \dots, \ell$ are the relaxation times and the dimensionless factors ω_i , $i = 1, \dots, \ell$ are material parameters. And where \mathbb{N} is the fourth-order tensor which depends solely on the Poisson's ratio ν . In Voigt engineering notation, this tensor is given by

$$\tilde{\mathbb{N}} = \frac{1}{(1+\nu)(1-2\nu)} \begin{bmatrix} 1-\nu & \nu & \nu & & & \\ \nu & 1-\nu & \nu & & & \\ \nu & \nu & 1-\nu & & & \\ & & & 1-2\nu & & \\ & & & & 1-2\nu & \\ & & & & & 1-2\nu \end{bmatrix} \quad (13)$$

where, and in all what follows, the tilde notation ($\tilde{\cdot}$) refers to matrix and vector representations of fourth- and second-order tensor quantities in Voigt notation, respectively.

Notice that, except for the case of a simple Kelvin-Voigt model with $\ell = 1$, the ℓ evolution equations (12) are all coupled since each single internal variable ε_i^y appears in all the ℓ equations. Notice also that if the ℓ factors ω_i are set to zero, then no viscous evolution takes place and the material response becomes elastic coupled to instantaneous damage.

And for the damage part of the material behaviour, the damage flow is given by an identical form as given for the unidimensional case, see (6)-(8). That is

$$\begin{cases} g(D; \varepsilon) = (1-D)^{m(D)} S(\varepsilon) - W \\ \dot{D} = \delta \\ \delta \geq 0, \quad g(D; \varepsilon) \leq 0, \quad \delta g(D; \varepsilon) = 0 \end{cases} \quad (14)$$

together with the consistency condition $\delta \dot{g}(D; \varepsilon)$, and where the exponent $m(D)$ is now given by the function (11).

Last but not least, as it is observed that damage within many rock-like materials is mostly produced by extensions, we choose the driving source of damage $S(\varepsilon)$ to depend on positive strain

quantities through the following volumetric energy form

$$S(\boldsymbol{\varepsilon}) = \frac{1}{2} \zeta_1 \boldsymbol{\varepsilon}^+ : \boldsymbol{\varepsilon}^+ + \frac{1}{2} \zeta_2 ((\text{tr}[\boldsymbol{\varepsilon}])^+)^2, \quad (15)$$

where the moduli ζ_1 and ζ_2 are material parameters, $\text{tr}[\cdot]$ designates the trace operator of second-order tensors, $\langle \cdot \rangle^+$ is the positive part scalar function as $\langle x \rangle^+ = \frac{1}{2}\{x + |x|\}$, and where the positive part $\boldsymbol{\varepsilon}^+$ of the *total* strain tensor $\boldsymbol{\varepsilon}$ is obtained after diagonalisation. In fact, as this latter is symmetric, its spectral decomposition is given as

$$\boldsymbol{\varepsilon} = \sum_{A=1}^3 \varepsilon_A \mathbf{n}^{(A)} \otimes \mathbf{n}^{(A)}, \quad (16)$$

where $\{\varepsilon_A\}_{A=1,2,3}$ are the principal strains with $\{\mathbf{n}^{(A)}\}_{A=1,2,3}$ being their corresponding principal directions. In (16), the symbol \otimes designates the tensor product. Hence $\boldsymbol{\varepsilon}^+$ is then expressed as

$$\boldsymbol{\varepsilon}^+ = \sum_{A=1}^3 \langle \varepsilon_A \rangle^+ \mathbf{n}^{(A)} \otimes \mathbf{n}^{(A)}, \quad (17)$$

and the source of damage function in (15) is then equivalently written as

$$S(\boldsymbol{\varepsilon}) = \frac{1}{2} \zeta_1 \{(\langle \varepsilon_1 \rangle^+)^2 + (\langle \varepsilon_2 \rangle^+)^2 + (\langle \varepsilon_3 \rangle^+)^2\} + \frac{1}{2} \zeta_2 ((\varepsilon_1 + \varepsilon_2 + \varepsilon_3)^+)^2. \quad (18)$$

Notice that this source of damage is general enough in the model at hand. It is decomposed into pure directional extensions' contribution in the first term, and a pure volumetric dilatency contribution in the second term. For simple compression tests, only the first term will contribute to damage evolution through the Poisson's ratio effect. However, the choice made for $S(\boldsymbol{\varepsilon})$ is not unique and alternative expressions can be used instead of (18). For instance, one can choose to make it depend solely on the deviatoric part of the total strain tensor if the material is more sensitive to shearing.

In summary: the phenomenological viscoelastic-damage model we use for the description of creep in natural gypsum rock is given by the constitutive equations (1)-(2), the ℓ viscoelastic evolution equations (12)-(13), and the damage flow equations (14) together with the definitions (11) and (18).

4. NUMERICAL INTEGRATION FOR THE LOCAL EVOLUTION EQUATIONS

In this section, we consider an algorithmic approximation consistent with the local evolution equations developed above. In a finite element context, this is accomplished at the integration points level through a strain-driven type of numerical procedure. Consider a typical time interval $[t_n, t_{n+1}]$, an arbitrary material point \boldsymbol{x} and assume that the variables $\boldsymbol{\varepsilon}_{i n}^v$, $i = 1 \dots \ell$ and D_n are known prescribed initial data on \boldsymbol{x} at time t_n . The objective is then to approximate the ℓ equations (12) and equations (14) to advance the solution to time t_{n+1} and update the variables to $\boldsymbol{\varepsilon}_{i n+1}^v$, $i = 1 \dots \ell$ and D_{n+1} for a fixed increment of deformation.

The key idea in the design of the integration algorithm is to exploit the fact that the ℓ viscoelastic evolution equations (12) are independent on the damage internal variable, on the one hand, and that the damage flow in (14) is independent on the viscous strain-like internal variables, on the other hand. This idea is then carried out simply by the combination of an algorithm adapted to the viscoelastic evolution and an algorithm adapted to the damage flow.

4.1. Implicit time integration of the viscoelastic part

Among other possibilities, we choose here the implicit backward-Euler scheme to approximate the evolution equations (12). This gives a linear system of ℓ coupled equations

$$\begin{aligned} \omega_i \Delta t \mathbb{N} : \varepsilon_{1n+1}^v &+ \dots + (\tau_i \mathbb{I} + (1 + \omega_i) \Delta t \mathbb{N}) : \varepsilon_{in+1}^v \\ &+ \dots + \omega_i \Delta t \mathbb{N} : \varepsilon_{\ell n+1}^v = \omega_i \Delta t \mathbb{N} : \varepsilon_{n+1} + \tau_i \varepsilon_{in}^v \end{aligned} \quad (19)$$

$i = 1, \dots, \ell$, where ε_{n+1} is the *known* total incremented strain tensor at time t_{n+1} , $\Delta t = t_{n+1} - t_n$ stands for the time increment, and where \mathbb{I} is the fourth-order symmetric unit tensor with components $I_{ijkl} = (\delta_{ik}\delta_{jl} + \delta_{il}\delta_{jk})/2$ with δ_{ij} being the Kronecker delta. For computational purposes, the ℓ equations (19) can be equivalently written in Voigt notation as

$$\mathbf{H} \begin{Bmatrix} \tilde{\varepsilon}_{1n+1}^v \\ \vdots \\ \tilde{\varepsilon}_{in+1}^v \\ \vdots \\ \tilde{\varepsilon}_{\ell n+1}^v \end{Bmatrix} = \begin{Bmatrix} \omega_1 \Delta t \tilde{\mathbb{N}} \tilde{\varepsilon}_{n+1} + \tau_1 \tilde{\varepsilon}_{1n}^v \\ \vdots \\ \omega_i \Delta t \tilde{\mathbb{N}} \tilde{\varepsilon}_{n+1} + \tau_i \tilde{\varepsilon}_{in}^v \\ \vdots \\ \omega_\ell \Delta t \tilde{\mathbb{N}} \tilde{\varepsilon}_{n+1} + \tau_\ell \tilde{\varepsilon}_{\ell n}^v \end{Bmatrix} \quad (20)$$

with \mathbf{H} being the matrix of the system given by

$$\mathbf{H} = \begin{bmatrix} \tau_1 \mathbb{I} + (1 + \omega_1) \Delta t \tilde{\mathbb{N}} & \dots & \omega_1 \Delta t \tilde{\mathbb{N}} & \dots & \omega_1 \Delta t \tilde{\mathbb{N}} \\ \vdots & & \vdots & & \vdots \\ \omega_i \Delta t \tilde{\mathbb{N}} & \dots & \tau_i \mathbb{I} + (1 + \omega_i) \Delta t \tilde{\mathbb{N}} & \dots & \omega_i \Delta t \tilde{\mathbb{N}} \\ \vdots & & \vdots & & \vdots \\ \omega_\ell \Delta t \tilde{\mathbb{N}} & \dots & \omega_\ell \Delta t \tilde{\mathbb{N}} & \dots & \tau_\ell \mathbb{I} + (1 + \omega_\ell) \Delta t \tilde{\mathbb{N}} \end{bmatrix}. \quad (21)$$

Notice that this latter matrix is constant and is the same for each integration point with the same material properties. Moreover, \mathbf{H} need to be computed, inverted and stored only once whenever the time increment Δt is kept constant during the incremental process.

4.2. Numerical integration for the damage flow

Within the same time interval $[t_n, t_{n+1}]$, the nowadays well known concept of ‘‘trial predictor/damage corrector’’ algorithm is applied to approximate the damage evolution given by the set of equations (14).

Within the trial prediction step, the damage flow is frozen and the criterion (14)₁ is evaluated for $D = D_n$ and $\varepsilon = \varepsilon_{n+1}$. That is

$$g_{n+1}^{\text{tr}} \equiv g(D_n; \varepsilon_{n+1}) = (1 - D_n)^{m(D_n)} S_{n+1} - W. \quad (22)$$

where $S_{n+1} \equiv S(\varepsilon_{n+1})$ is a known quantity obtained by mere function evaluation of the source of damage function (18) at ε_{n+1} . S_{n+1} is considered fixed at this level. Hence, two situations can occur:

- if $g_{n+1}^{\text{tr}} \leq 0$, then the trial state is admissible and we set $D_{n+1} = D_n$.
- else if $g_{n+1}^{\text{tr}} > 0$, then a damage flow process is taking place and a damage correction has to be performed.

For the damage model at hand, the damage correction procedure is simply accomplished by solving $g_{n+1} \equiv g(D_{n+1}; \varepsilon_{n+1}) = 0$ for D_{n+1} . Moreover, using the natural logarithm leads to an equivalent equation

$$m(D_{n+1}) \ln(1 - D_{n+1}) = \ln \left[\frac{W}{S_{n+1}} \right]. \quad (23)$$

This nonlinear equation can be solved locally by means of a Newton iterative procedure as summarized in Table I.

4.3. Algorithmic tangent moduli

The initial boundary value problem of gypsum creep is nonlinear. The source of nonlinearity is a material one which arises from the constitutive relation. Hence, this problem is solved by means of an iterative process of the Newton's type. Accordingly, this requires the linearization of the global equilibrium problem about a known state at time t_n . This procedure is nowadays standard. We give here the contribution to the algorithmic tangent stiffness where it is of interest to determine the relation between the rate of stress and the rate of *total* strain via the algorithmic change of the internal variables ε_i^v , $i = 1, \dots, \ell$ and D .

We start from the rate form of the constitutive relation (1) by taking into account the additive decomposition (2). One obtains

$$\dot{\sigma} = (1 - D) E \mathbb{N} : (\dot{\varepsilon} - \dot{\varepsilon}_1^v - \dots - \dot{\varepsilon}_\ell^v) - \dot{D} \sigma_0 \quad (24)$$

where $\sigma_0 = \mathbf{C} : (\varepsilon - \varepsilon^v)$ denotes the effective stress tensor and where use has been made in (24) of the fact that the isotropic Hooke's elasticity tensor can be written as $\mathbf{C} = E \mathbb{N}$ where the Poisson's ratio's dependent fourth-order tensor \mathbb{N} has been defined in (13), and where the scalar material parameter E is the elastic Young's modulus.

On the one hand, from the discrete form (20), we deduce the algorithmic rate of change of the internal variables ε_i^v , $i = 1, \dots, \ell$, in terms of the rate of change of the total strain ε . In matrix form, this is given by

$$\begin{Bmatrix} \dot{\varepsilon}_1^v \\ \vdots \\ \dot{\varepsilon}_\ell^v \end{Bmatrix} = \mathbf{H}^{-1} \begin{bmatrix} \omega_1 \Delta t \tilde{\mathbb{N}} \\ \vdots \\ \omega_\ell \Delta t \tilde{\mathbb{N}} \end{bmatrix} \dot{\varepsilon}. \quad (25)$$

Table I. Local damage update.

If $g_{n+1}^{\text{tr}} > 0$ then perform the following correction procedure

1. Initialize: $k = 0, D_{n+1}^{(0)} = D_n$
2. Evaluate residual and check convergence

$$r_{n+1}^{(k)} = \ln \left[\frac{W}{S_{n+1}} \right] - m_{n+1}^{(k)} \ln(1 - D_{n+1}^{(k)})$$

$$\text{with } m_{n+1}^{(k)} = m_1 (1 - D_{n+1}^{(k)})^{m_2} + m_3$$

IF $|r_{n+1}^{(k)}| > TOL$ THEN go to Step 3

ELSE set $D_{n+1} = D_{n+1}^{(k)}$ and EXIT.

3. Compute the damage increment

$$\text{set } \alpha_{n+1}^{(k)} = m_{n+1}'^{(k)} \ln(1 - D_{n+1}^{(k)}) - \frac{m_{n+1}^{(k)}}{1 - D_{n+1}^{(k)}}$$

$$\text{with } m_{n+1}'^{(k)} = -m_1 m_2 (1 - D_{n+1}^{(k)})^{m_2 - 1}$$

$$\Delta D_{n+1}^{(k)} = \frac{r_{n+1}^{(k)}}{\alpha_{n+1}^{(k)}}$$

4. Update

$$D_{n+1}^{(k+1)} = D_{n+1}^{(k)} + \Delta D_{n+1}^{(k)}$$

Set $k \leftarrow k + 1$ and return to Step 2.

And, on the other hand, the rate form of the damage consistency equation (23) gives the following rate of change of the damage variable D in terms of the rate of change of the total strain ε

$$\dot{D} = - \frac{1}{\alpha(D) S(\varepsilon)} \frac{\partial S(\varepsilon)}{\partial \varepsilon} : \dot{\varepsilon} \quad (26)$$

with the notation (see also Table I, step 3) $\alpha(D) = m'(D) \ln(1 - D) - m(D)/(1 - D)$.

Then, in Voigt notation, the algorithmic tangent moduli are given in matrix form as

$$\tilde{\mathbf{C}}_T^{\text{algo}} = (1 - D)E \left(\tilde{\mathbf{N}} - \underbrace{\begin{bmatrix} \tilde{\mathbf{N}} & \dots & \tilde{\mathbf{N}} \\ \ell \text{ times} \end{bmatrix}}_{\ell \text{ times}} \mathbf{H}^{-1} \begin{bmatrix} \omega_1 \Delta t \tilde{\mathbf{N}} \\ \vdots \\ \omega_\ell \Delta t \tilde{\mathbf{N}} \end{bmatrix} \right) + \frac{1}{\alpha(D) S(\varepsilon)} \left[\tilde{\boldsymbol{\sigma}}_0 \otimes \frac{\partial \tilde{S}}{\partial \varepsilon} \right] \quad (27)$$

such that $\dot{\boldsymbol{\sigma}} = \tilde{\mathbf{C}}_T^{\text{algo}} \dot{\varepsilon}$.

Now it only remains to precise the expression of the symmetric second-order tensor $\partial S / \partial \varepsilon$. As the source of damage function given by (18) is of the form $S = S(\varepsilon_1, \varepsilon_2, \varepsilon_3)$, by the chain rule

together with the spectral decomposition (16), one obtains

$$\frac{\partial S}{\partial \boldsymbol{\varepsilon}} = \sum_{A=1}^3 \frac{\partial S}{\partial \varepsilon_A} \mathbf{n}^{(A)} \otimes \mathbf{n}^{(A)}, \quad (28)$$

where the important spectral property

$$\frac{\partial \varepsilon_A}{\partial \boldsymbol{\varepsilon}} = \mathbf{n}^{(A)} \otimes \mathbf{n}^{(A)}, \quad A = 1, 2, 3 \quad (29)$$

has been used. And finally, with the other useful property relative to the positive part function that

$$\frac{\partial \langle x \rangle^+}{\partial x} \langle x \rangle^+ = \langle x \rangle^+ \quad (30)$$

for any scalar x , we end up with the following expression

$$\frac{\partial S}{\partial \varepsilon_A} = \zeta_1 \langle \varepsilon_A \rangle^+ + \zeta_2 \langle \varepsilon_1 + \varepsilon_2 + \varepsilon_3 \rangle^+, \quad A = 1, 2, 3. \quad (31)$$

5. REPRESENTATIVE NUMERICAL EXAMPLES

As an illustration of the modelling framework developed in this paper, we give in this section numerical examples of gypsum creep simulated within the context of the finite element method.

To identify the parameters of the viscoelastic-damage model at hand from laboratory tests we proceed in two steps. In the first step, we capture the short-term behavior of the material when no creep takes place. Roughly speaking, in this case, only the elastic-damage free spring is activated in the rheological model of Figure 2, while the ℓ Kelvin elements are kept frozen. In fact, we admit that the characteristic relaxation times are large enough compared to the duration of monotonic tests. This permits to identify the elastic and the damage parts of the material parameters: the Young's modulus E , the Poisson's ratio ν , the initial damage threshold W , the parameters of the exponent function m_1 , m_2 and m_3 , and the source of damage parameters ζ_1 and ζ_2 . For instance, curve fitting can be used from experimental test results in compression. And, in the second step, creep tests have to be performed at different levels of loading to capture the complementary material parameters relative to the viscous behavior. Curve fitting can also be used to capture one or more characteristic times ($\ell \geq 1$) together with the corresponding parameters: (τ_i, ω_i) , $i = 1 \dots \ell$.

After [1], the strength in compression of saccharoid gypsum in saturated condition varies between 13.7 and 23.5 MPa, while the Young's modulus is found to vary between 6900 and 9100 MPa. This natural gypsum rock is of macrocrystalline type with mean crystal dimensions varying between 0.1 and 1 mm. Now, and in the absence of experimental results under monotonic tests, we postulate a ductile response in compression. The short-term behavior we use in the following computations is given by the simulated curve illustrated in Figure 3.

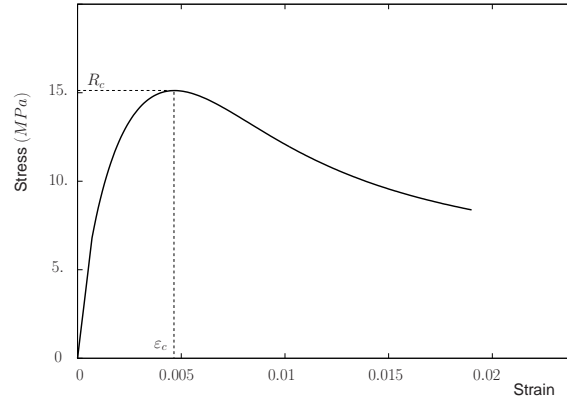


Figure 3. Short-time behavior. Stress-strain curve in simple compression.

The material parameters used to obtain this stress-strain relation in compression are

$$\begin{aligned} E &= 9000 \text{ MPa}, & \nu &= 0.27, \\ W &= 0.75 \cdot 10^{-4} \text{ MPa}, & m_1 &= 4, & m_2 &= 0.8, & m_3 &= 1.8, & \zeta_1 &= 2250 \text{ MPa}. \end{aligned} \quad (32)$$

And the resulting strength in compression is $R_c = 15.12 \text{ MPa}$. Two important observations must be pointed out:

- To obtain the result of Figure 3, the partial set of parameters (32) has been chosen such that the strain at the pic-load ε_c coincides more or less with the total strain that initiates the tertiary creep in Figure 1. Here we have $\varepsilon_c = 4.7 \cdot 10^{-3}$.
- If, for example, the compressive load direction coincides with the global \vec{e}_1 -axis, the principal strain ε_1 is then negative while the other two principal strains are equal and positive due to the Poisson's ratio effect

$$\varepsilon_1 < 0, \quad \text{and} \quad \varepsilon_2 = \varepsilon_3 = -\nu \varepsilon_1 > 0. \quad (33)$$

Then, in view of the expression of the driving source of damage function $S(\varepsilon)$ in (18), the volumetric strain ($\varepsilon_1 + \varepsilon_2 + \varepsilon_3$) is negative in this case and the material response is independent on the material parameter ζ_2 .

5.1. Long-term creep tests

In this example, a series of creep tests are computed using the precedent (*instantaneous*) elastic-damage behavior with different levels of the load in compression. Besides on the material parameters (32), we choose to activate three viscoelastic mechanisms with the following couples of parameters

$$(\tau_1 = 20 \text{ h}, \omega_1 = 0.9) \quad (\tau_2 = 100 \text{ h}, \omega_2 = 0.5) \quad (\tau_3 = 1000 \text{ h}, \omega_3 = 0.2) \quad (34)$$

The Figure 4 gives a set of simulated axial strain curves versus time up to 14400 h (about 600 days) for the lowest load. On the one hand, we obtain the typical S-shaped curves highlighting the three stages corresponding to the primary transient creep, the secondary pseudo-linear creep, and the fast tertiary creep before failure. And on the other hand, one can check that the tertiary creep initiates at strains of the order of the pic-strain ε_c .

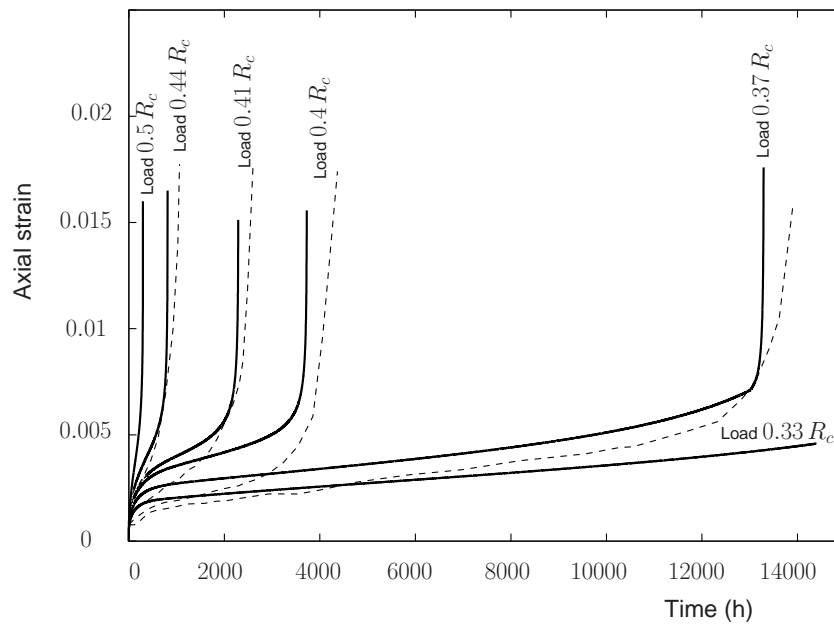


Figure 4. Axial strain curves versus time for simulated creep tests under different levels of loading (solid lines). Superposition with experimental results of Figure 1 for 0.37, 0.4, 0.41 and 0.44 R_c (dashed lines).

Having in mind that there are almost always dispersions in laboratory data at least due to dispersion of rock properties, there is qualitatively and, to a lesser extent, quantitatively good accordance with the experimental results of Figure 1. Finally, and as an illustration, Figure 5 shows the corresponding *hidden damage* evolutions predicted by the viscoelastic-damage model.

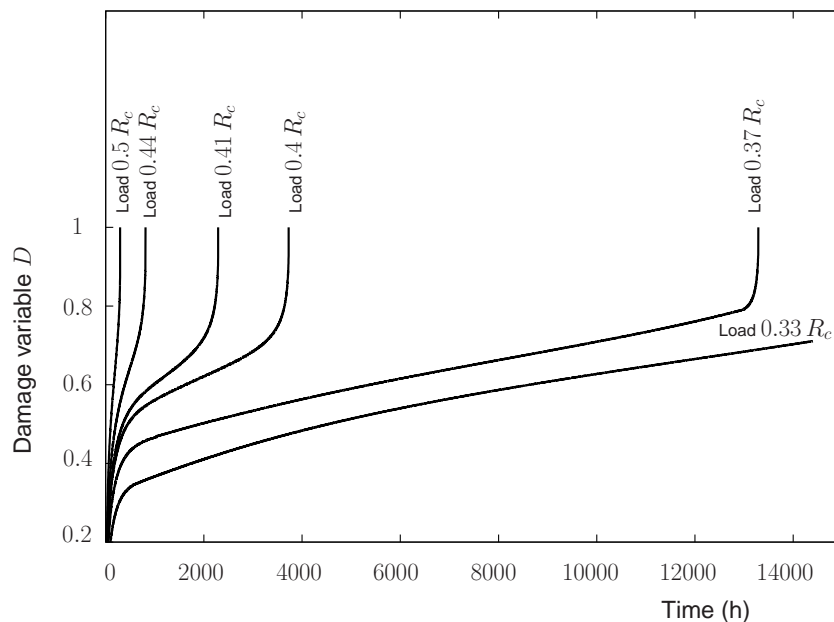


Figure 5. Corresponding damage evolutions during the creep tests under different levels of loading.

5.2. Multi-step creep tests

To gain further insight into the present model, we simulate in this section various multi-step creep tests. The material data used are those of the precedent example given by (32) and (34).

Figure 6 shows the strain curves versus time for different loading histories. First of all, notice from Figure 4 that the complete failure for a constant compressive creep load of value $0.4 R_c$ is reached at time $t = 3725 h$. We next observe that a reduction of this stress to a value of $0.33 R_c$ at various terms produce marked differences in the material response. In fact, the material degradation is almost stabilized for the test duration when the load is dropped at early terms, while beyond a threshold term where a certain limit deformation has been reached, this load reduction does not preclude failure, but delays it of some thousands or decades of hours.

Hence, with the present model, the gypsum rock would consequently have different responses depending on the loading conditions applied in its natural underground mining environment and with regards to the influence of the recovery duration representing the delayed time between the in situ sampling and the laboratory tests.

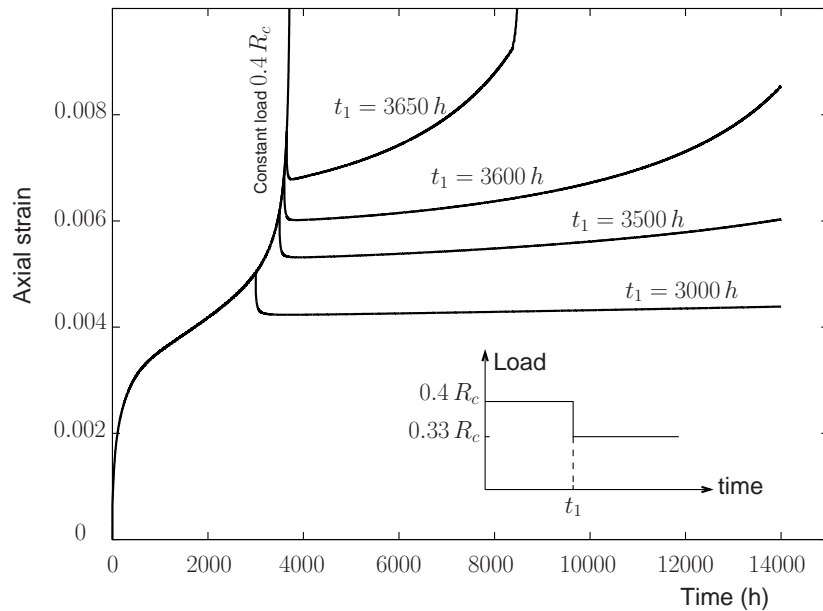


Figure 6. Multi-step creep tests. Loading histories and axial strain evolutions for different terms at $t_1 = 3000, 3500, 3600$ and $3650 h$. The strength in compression is $R_c = 15.12 MPa$.

Moreover, for perfectly identical loading histories but reversed, the material response differs significantly. In other words, the response is greatly influenced by the order of application of the loads for the same loading durations. This property is illustrated in the example of Figure 7 where the following two loading histories have been applied: The first one with a compression of value $0.4 R_c$ up to time $t_1 = 2800 h$ followed by a drop to the load of value $0.3 R_c$ until time $t_2 = 5600 h \equiv 2 t_1$. And the second one with a compression of value $0.3 R_c$ up to time $t = t_1$ followed by a jump to the load of value $0.4 R_c$ until time $t = t_2$. One can observe that the two strains at the end of the tests are very different. The latter is reaching failure while the former is almost stabilized.

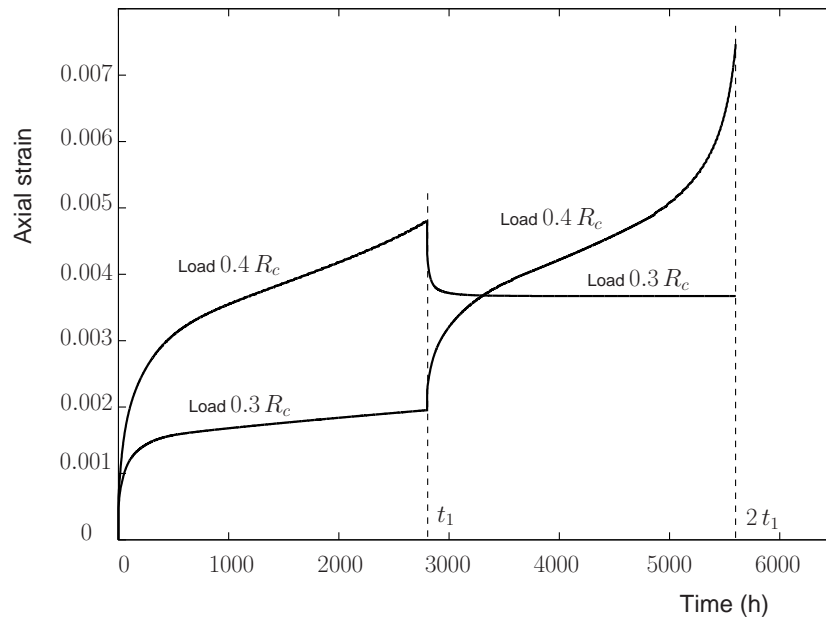


Figure 7. Multi-step creep tests with reversed loading histories at $t_1 = 2800 h$. Axial strain evolutions for the two loading histories. The strength in compression is $R_c = 15.12 MPa$.

6. CONCLUSIONS

The main thrust of this paper has been the presentation of a model in order to provide a tool for the prediction of the long-term creep in gypsum rock materials. The model developed is based on the nowadays well known continuum damage mechanics framework.

The material response has been captured with the coupling between a local damage model based on the yield surface concept, and a generalized Kelvin-Voigt rheological model. Each of them has been deeply investigated and motivated by experimental observations. In particular for the viscoelastic part, the model can integrate as many as necessary viscoelastic processes with different relaxation times.

A detailed algorithmic treatment has been developed to numerically integrate the constitutive law together with the evolution equations within a finite element procedure. Due to the nature of the *local* evolution equations, an algorithm adapted to the viscoelastic evolution has been combined with a return mapping algorithm adapted to the damage flow. And the algorithmic tangent moduli have been given in order to numerically solve the *global* nonlinear initial boundary value problem by a Newton-like iterative procedure.

It has been shown through a set of numerical examples that the present model is able to capture the long-term creep response of natural gypsum rock materials. A good accordance with experimental results on saccharoid gypsum under saturated conditions found in the literature has been obtained. Notice that saturated conditions correspond to an upper creep bound. And finally, numerical simulations with different loading histories have exhibited surprising long-term responses that should be investigated more deeply from the experimental point of view.

REFERENCES

1. Moirat D, Potherat P, Massieu E, Durville JL. Experimental data on creep of the saccharoid gypsum in saturated condition. *Revue Française de Géotechnique* 2006; **115**:3–10.
2. Hoxha D, Giraud A, Homand F. Modelling long-term behaviour of natural gypsum rock. *Mechanics of Materials* 2005; **37**(12):1223–1241.
3. Chen Z, Wang ML, Lu T. Study of the tertiary creep of rock salt. *Journal of Engineering Mechanics (ASCE)* 1997; **123**(1):233–242.
4. Yahya OML, Aubertin M, Julien MR. A unified representation of plasticity, creep and relaxation behaviour of rock salt. *International Journal of Rock Mechanics and Mining Science* 2000; **37**:787–800.
5. Le Roy R, Granger L. Calcul des déformations instantanées et de fluage propre du béton à partir de celles de la pâte de ciment. *Bulletin de Liaison des Laboratoires des Ponts et Chaussées* 1995; **196**:67–78.
6. Schapery RA. Nonlinear viscoelastic and viscoplastic constitutive equations with growing damage. *International Journal of Fracture* 1999; **97**:33–66.
7. Suvorova JV, Ohlson NG, Alexeeva SI. An approach to the description of time dependent materials. *Materials and Designs* 2003; **24**:293–297.
8. Torrenti JM, Nguyen VH, Colina H, Le Maou F, Benboudjema F, Deleruyelle F. Coupling between leaching and creep of concrete. *Cement and Concrete Research* 2008; **38**:816–821.
9. Nedjar B. Elastoplastic-damage modelling including the gradient of damage. Formulation and computational aspects. *International Journal of Solids and Structures* 2001; **38**:5421–5451.
10. Nedjar B. A theoretical and computational setting for geometrically nonlinear damage modelling framework. *Computational Mechanics* 2002; **30**:65–80.
11. Simo JC, Ju JW. Strain- and stress-based continuum damage models - I. Formulation. *International Journal of Solids and Structures* 1987; **23**:821–840.